

# High Refractive Index Fluid Evaluations at 193 nm: Fluid Lifetime and Fluid/Resist Interaction Studies

Hoang V. Tran<sup>a</sup>, Eric Hendrickx<sup>b</sup>, Roger H. French<sup>a</sup>, Douglas J. Adelman<sup>a</sup>,  
Nyrisa S. Rogado<sup>a</sup>, Mureo Kaku<sup>c</sup>, Michael Mocella<sup>d</sup>, John J. Schmieg<sup>d</sup>,  
Charles Y. Chen<sup>e</sup>, Frieda Van Roey<sup>b</sup>, Adam S. Bernfeld<sup>a</sup>, Rebekah A. Derryberry<sup>a</sup>

<sup>a</sup>DuPont Central Research and Development, Wilmington, DE 19880-0500

<sup>b</sup>IMEC, Kapeldreef 75, B3001 Leuven, Belgium

<sup>c</sup>DuPont K. K., NBD-J, Utsunomiya-shi, Japan, 321-3231

<sup>d</sup>DuPont Electronic Technologies, Wilmington, DE 19880

<sup>e</sup>DuPont-EKC, Hayward CA, 94545

We report on recent studies on two of our leading fluid candidates for high index immersion lithography, designated IF132 and IF169. The most recent fluid radiation durability results are discussed, leading us to define two important parameters, the fluid lifetime factor and the clean window dose related to suppression of window contamination through use of active recycle technology. Results of fluid-resist interactions, with water and high index fluids on four commercial resists, will be shown. These experiments include PAG leaching and contact angle measurements, resist profile and thickness changes due to pre- and post-exposure fluid contact, residues and defects from the fluid and from resist contact, and 36 nm hp imaging on an immersion interference printer.

**Keywords:** immersion lithography, second generation fluid, refractive index, absorbance, radiation durability, active recycle, window contamination, leaching, resist/fluid interactions, defectivity

## 1. Introduction

Three distinct lithographic technologies are now being readied for manufacturing insertion in the foreseeable (1-7 years) future. These technologies – water immersion double patterning, high index immersion (in both single-exposure and double-patterning variations) and EUV – are commonly considered competing technologies, but may actually be best viewed as complementary, and thus mutually supporting, to achieve the industry's overall technology goals.

Water-based immersion lithography's emergence enabled half-pitch resolutions to below 40 nm, a level not achievable by dry 193 nm illumination methods, and so extended the utility of the current leading-edge imaging wavelength (Figure 1). By adopting methods such as the various double-patterning options, this approach could extend to perhaps 26 nm or even less – meeting the most-demanding near-term user requirements for memory technologies in particular. These water-immersion extensions have allowed more time for the other two technologies to develop; and at present, high-index immersion would be the next likely

technology. With high index lithography the aggressive k1 values needed for water double patterning can be relaxed. At the same time, returning to a single-exposure method is expected to provide the cost and throughput advantages which are generally obtained versus a double-patterning approach [1].

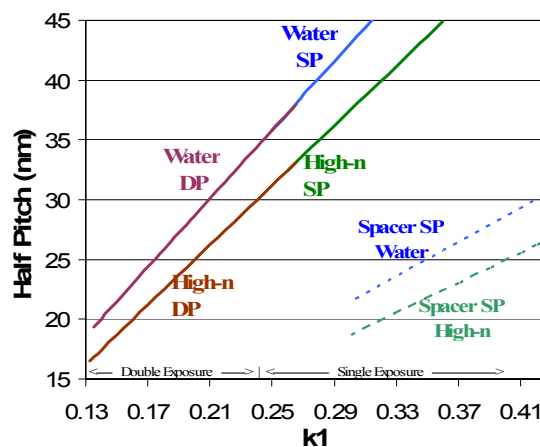


Figure 1. Half pitch versus k1 for water, high index fluid, and spacer technology single patterning (SP) and double patterning (DP).

The next patterning approach is presently unclear. If EUV is ready with acceptable cost of ownership, it would be inserted due to the extendibility advantages it offers versus the other two approaches. However, the multiple unresolved technical issues in EUV – including notably tool development, an illumination source of sufficient power, a mature mask production and inspection infrastructure, and photoresists with acceptable combinations of sensitivity, resolution and line edge roughness – suggest that interim approaches will be required. In such a case, the experience gained in double-patterning approaches with water can form the basis for similar high-index methods, enabling half pitches approaching 16 nm to be realized with the most aggressive k1 reductions. In this way, the full EUV infrastructure can develop over a period more suitable for the major process and materials shifts which accompany any patterning wavelength change.

To support these transitions, we are continuing our work to develop the fluid and associated technologies for high-index immersion, to ensure their readiness as needed in the full set of lithographic options [2-10]. We report here on selected aspects of this ongoing work, including high-index fluid issues comprising fluid radiation durability, fluid recycle technology, window darkening rates, fluid quality and handling, and fluid/resist interactions.

## 2. Fluid Lifecycle: Radiation Durability and Active Recycle

### 2.1. Typical Fluid and Window Radiation Durability Doses

Radiation durability studies must meaningfully relate to the conditions found in modern lithographic tools. We have previously reported on the development of the Standard Stepper Tool, whereby experimental radiation durability studies could be properly related to commercial stepper/scanner conditions. [9] In Figure 2, the Standard Stepper Tool is used for the “Stepper Down” Perspective: using typical stepper parameters, and reasonable immersion fluid values, to define doses for both the immersion fluid as well as the final lens element in contact with the fluid (“window”). An alternative approach is the “Wafer Up” Perspective: using typical resist parameters and throughput conditions to define the dose values. These two perspectives are considered to reasonably bracket the conditions which will be encountered in actual practice, which will of course vary among tools

and users. As a starting point based on the values shown, we define “typical” values of 60 kJ/cm<sup>2</sup> for the daily window dose, and 6 J/cm<sup>2</sup> for the weekly fluid dose.

### Expose A Day's Wafers: What Is The Delivered Dose?

“Stepper Down” Perspective	“Wafer Up” Perspective
<ul style="list-style-type: none"> <li>• 6 kHz, 0.8 mJ/cm<sup>2</sup>/pulse Laser</li> <li>• 29mm x 7 mm Slot, 0.5 Duty Cycle</li> <li>• 1.568 mJ/pulse</li> <li>• For 3 mm Fluid Thickness</li> <li>• And 100 liter Reservoir</li> </ul>	<ul style="list-style-type: none"> <li>• For A Resist Sensitivity Of 30 mJ/cm<sup>2</sup></li> <li>• 3000 Wafers Per Day</li> <li>• 300 mm Wafers</li> <li>• For 3mm Fluid Thickness</li> <li>• And 100 Liter Reservoir</li> </ul>
<b>Total Daily Laser Dose = 406 kJ/Day</b>	<b>Total Daily Laser Dose = 64 kJ/Day</b>
<b>Total Window Dose = 207 kJ/cm<sup>2</sup></b>	<b>Total Window Dose = 34 kJ/cm<sup>2</sup></b>
<b>Fluid Dose Is 1.2 J/cm<sup>2</sup></b>	<b>Fluid Dose Is 0.2 J/cm<sup>2</sup></b>
<div style="border: 1px solid red; padding: 5px; display: inline-block;"> <p>“Typical” Estimates 60 kJ/cm<sup>2</sup> Window Dose Per Day 6 J/cm<sup>2</sup> Fluid Dose Per Week</p> </div>	

#### Real Values Dependent On Many Factors

• Since Stepper And Lithography Process Are “Owned” By Others

Figure 2. Fluid handling system with active recycle technology used for radiation durability testing.

### 2.2. Improvements in Active Recycle: Reducing the Induced Fluid Absorbance Rate

The experimental procedures for determining induced window and fluid absorbance increases (“darkening rates”) have been previously reported. [9] Our principal fluid candidate, IF132, has a natural (i.e., in the absence of active recycle) darkening rate of 0.079 J/cm, determined over many experiments (Figure 3). With early versions of our active recycle package (ARP) technology, this darkening rate could be significantly reduced. Versions 3 and 4 of active recycle technology gave Fluid Lifetime Factors (i.e., darkening rate ratio for no ARP, versus with ARP) in the range of 3-9 (Figure 4).

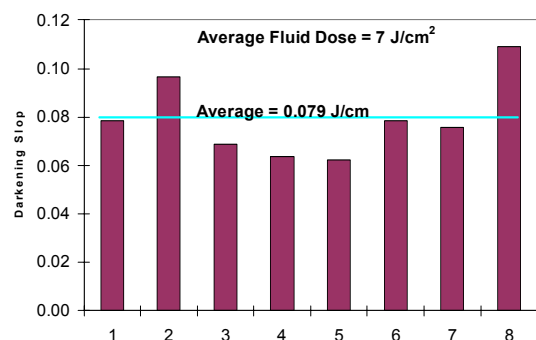


Figure 3. Induced fluid absorbance rate (darkening rate) for IF132 without the use of Active Recycle.

We continue to optimize this technology, with version 5 active recycle now giving a Fluid Lifetime Factor of 15 (Figure 5). The exact translation of this factor into usable fluid life

depends on the upper permissible tool limit of fluid absorbance. However, based on our typical initial fluid absorbances of 0.03/cm, and an assumed upper absorbance limit of 0.10/cm, this result indicates the capability of week long fluid use at acceptable absorbance values.

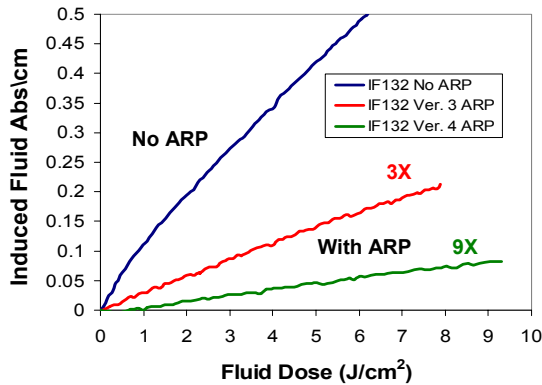


Figure 4. Induced fluid absorbance versus fluid dose for IF132 with No ARP, v3 and v4 ARP.

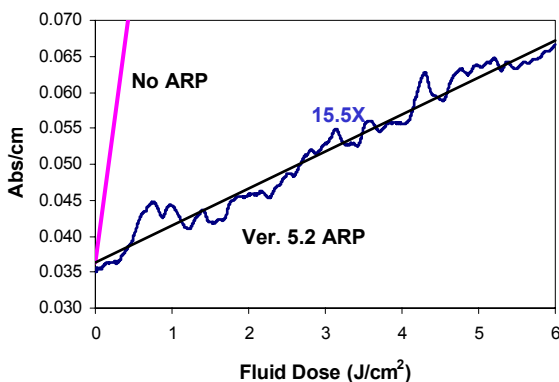


Figure 5. Total fluid absorbance versus fluid dose for IF132 with No ARP and v 5.2 ARP.

### 2.3. Active Recycle For Suppression Of Window Contamination

Successful active recycle technology must not only suppress fluid degradation, but must also minimize increases in final lens element absorbance due to the fluid-lens contact under 193 nm illumination. Figure 6 compares the induced window absorption for a version 4 ARP versus a no ARP case. In the ARP's absence, the induced window absorbance increases at a greater-than-linear rate over the range studied. In contrast, with the ARP, there was an induction (or suppression) period in which no increase in window absorption was seen up to a dose of about 6 kJ/cm<sup>2</sup>, and a roughly linear increase thereafter over the range studied. Thus, the ARP suppressed the window contamination to a window dose of 6 kJ/cm<sup>2</sup>. We define the Clean Window Dose as the window

dose below which the induced window absorbance is below 0.005/cm, and this suppression period corresponds to a few hours of window/lens use before the upper limit is reached. Further studies are underway to increase this value, and there are preliminary indications that active recycle technology can lead to clean window doses of 50 kJ/cm<sup>2</sup> corresponding to at least a day's use.

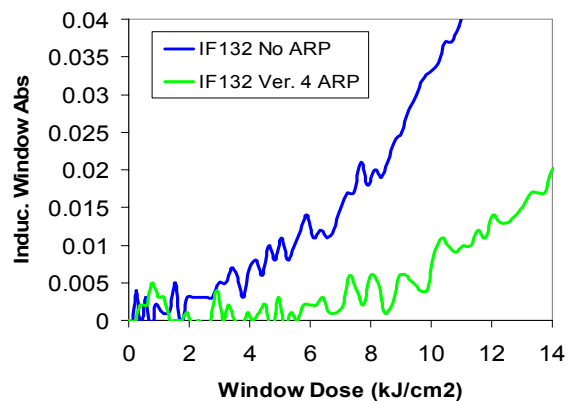


Figure 6. Induced window absorbance versus window dose for IF132 with No ARP and with v4 ARP.

## 3. Fluid Quality and Handling

### 3.1. Particles and Residues

Our efforts continue on the elimination of both soluble and insoluble impurities, to obtain ultrapure high-index liquids. For example, during testing to find the most compatible and efficient filters for IF132 (our leading high-index immersion fluid candidate), we have found that filters vary in their ability to remove insoluble particles, and that some add additional soluble contaminants. Some of these soluble contaminants do not reduce fluid transparency at 193 nm, so we have focused on droplet and misting tests to determine the filtered fluids' cleanliness.

Residue analysis tests involved manually dispensing droplets (1-5 mm in diameter) onto prewashed bare Si wafers, then monitoring the droplets' room temperature evaporation in a clean room environment with a LEXT confocal microscope. IF132 droplets in this size range require hours to completely evaporate at room temperature; therefore, evaporation was accelerated by heating the wafers until the droplets were ~500 μm in diameter, and further evaporation was then monitored at room temperature. Residues were counted, their areas tabulated, and the final residue volume percent

calculated based on the initial droplet volume. The details of this analysis method are significant, and so are included here.

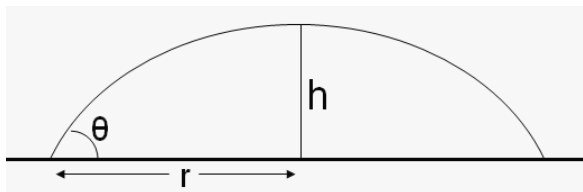


Figure 7. Diagram of a cross-section of a droplet/dome showing height,  $h$ , radius,  $r$ , and contact angle,  $\theta$ .

A sessile droplet's volume on a wafer is determined using Equation 1, where Figure 7 shows the relevant sessile droplet parameters: radius  $r$ , height  $h$ , and contact angle  $\theta$ .

$$\text{Equation 1. } V = \frac{1}{6} \pi \tan \theta (3 + \tan^2 \theta) r^3$$

To determine the fluid's residue volume fraction, the residues were analyzed using an Olympus LEXT OLS 3100 (Olympus Surgical and Industrial America Inc, Micro-Imaging Division, One Corporate Drive, Orangeburg, NY 10962) and the LEXT OLS software. Projected residue areas on a wafer are generated for each individual residue using the LEXT analysis software; the projected residue area,  $A$ , corresponds to the radius,  $r$ , of a sessile droplet as shown in Equation 2.

$$\text{Equation 2. } r^2 = \frac{A}{\pi}$$

Substituting Equation 2 into Equation 1, the volume of a single residue can be found using Equation 3.

$$\text{Equation 3. } V = \frac{1}{6} \pi \tan \theta (3 + \tan^2 \theta) \left( \frac{A}{\pi} \right)^{3/2}$$

The volume fraction  $V\%$  of all residues present in a fluid sessile droplet is found by dividing the summed residue volumes  $V_{R,i}$  by the initial sessile droplet volume  $V$ , as shown in Equation 4.

$$\text{Equation 4. } V\% = \frac{\sum_i V_{R,i}}{V}$$

Residue volume fractions are calculated using

Equation 5, assuming the same contact angles for the residues and the initial fluid droplet, and substituting Equation 1 and Equation 3 into Equation 4 for the initial sessile droplet volume  $V$ , and the residue volumes  $V_{R,i}$ , respectively.

$$\text{Equation 5. } V\% = \frac{\sum_i (A_i^{3/2})}{r^3 \pi^{3/2}}$$

In Equation 5,  $A_i$  is the individual projected areas of the residues detected and  $r$  is the radius of the initial sessile droplet.

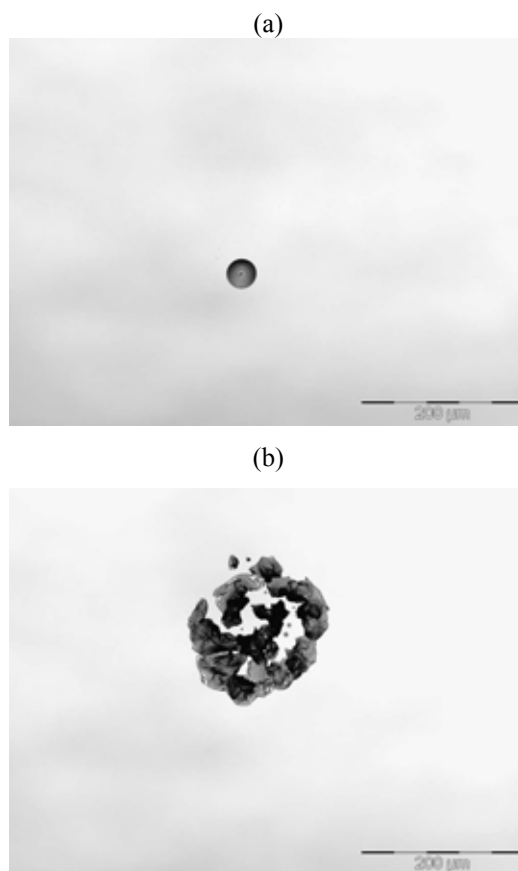


Figure 8. Final confocal image of an IF132 droplet (a) evaporated on a bare Si wafer for 15 minutes, compared to (b) a droplet of IF132 that has been filtered through a Whatman PTFE 0.45  $\mu\text{m}$  filter.

Figure 8 shows the final image of an IF132 droplet evaporated on a bare Si wafer for about 15 minutes, compared to the same fluid that was first filtered through a Whatman PTFE 0.45  $\mu\text{m}$  filter. The initial fluid showed a calculated 100 ppb residue, while the filtered droplet corresponded to more than 1 ppm residue. Figure 9 shows the initial fluid's absorbance spectrum, compared to those filtered through two filter types. As can be seen, materials of construction such as filters can

not only introduce particles and insoluble residues, but may also add soluble contaminants which increase fluid absorbance. Therefore, it is important to select materials which minimize fluid contamination, and also to implement an active recycle technology to remove these contaminants. Of course, the active recycle technology must also control use-generated contaminants, such as those from fluid contact with the resist and/or topcoat, and fluid degradation products resulting from 193 nm illumination.

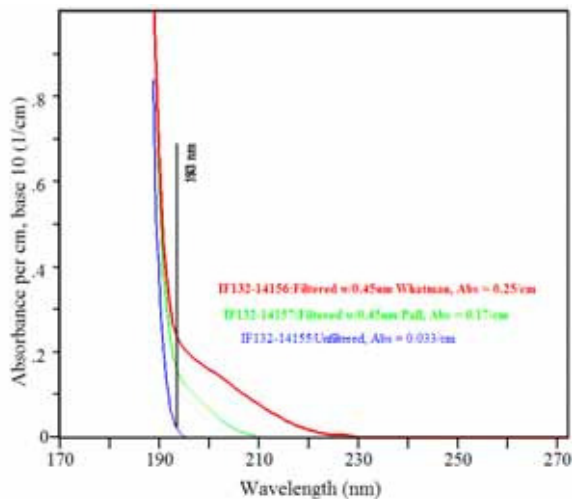


Figure 9. Absorbance of clean, unfiltered fluid compared to fluid that has been filtered through two types of filters.

#### 4. Fluid-Resist Interactions

Building on previous studies [8] of high index fluid/resist interactions on Sumitomo PAR-817 dry line-space resist, we now have additional data on three water-specific immersion resists – a TOK TARF-Pi6-001 resist (line-space), a TOK TAI-series resist (line-space), and a water-specific contact hole (CH) resist. Advancing and receding contact angles of the fluids were recorded on each resist. Misting experiments were performed to test both initial fluid cleanliness on bare Si wafers, as well as additional defects upon direct fluid-resist contact. PAG leaching into both water and the high index fluids were compared among the resists. Tests were also performed to compare the fluids’ effects on resist profile changes in pre-exposure and post-exposure soak modes, using scatterometry metrology. Finally, 72 nm half pitch lines were imaged using an immersion interference printer.

##### 4.1. Contact Angles

Contact angles were measured directly on each resist surface without using any topcoat. As

shown in Figure 10, both the advancing and receding contact angles of the high index fluids are substantially lower than that of water. The improvements made to increase the contact angles for water in the water-specific immersion resists also seem to help with the advancing angles on high index fluids, but does not improve the receding angles. This will impact the showerhead design for high index fluids, and schemes to remove residual fluid will be necessary if a “partially wet” showerhead design is chosen. Optimization of existing water-immersion topcoats for use with high index fluids, or design of new topcoatless resists for high index fluids, may be required.

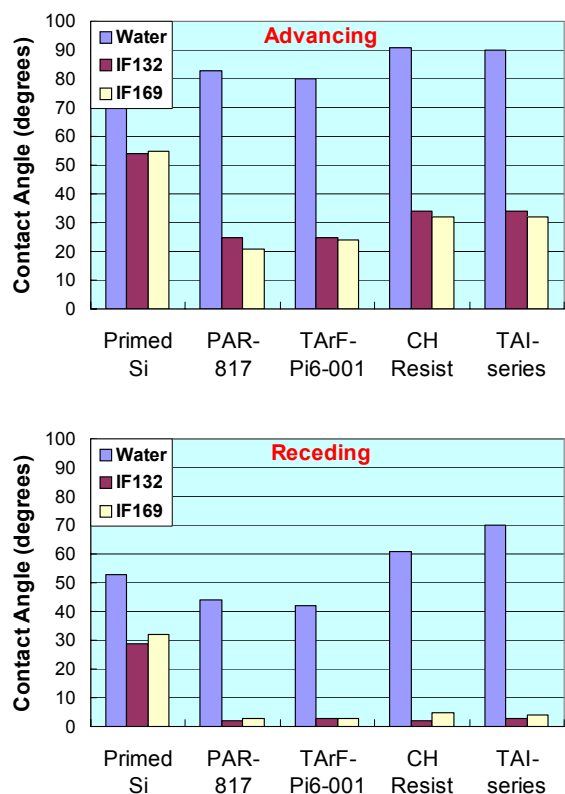


Figure 10. Advancing and receding contact angles of water, IF132, and IF169 on primed Si, a dry resist, and three water-specific immersion resists.

##### 4.2. Defectivity from Fluid Misting

A glass reagent sprayer (CAMAG) was used to mist thousands of high index fluid droplets onto bare Si wafers and resist-coated wafers. The droplets were air dried, and defects measured on a KLA SP1 Surfscan defect inspection tool. Defects present before misting were subtracted. A control experiment was also performed to test the sprayer’s cleanliness, where a blank Si wafer was sprayed only with air; about 50 added defects (the base background level) were found. Note

that we found the defect counts to greatly depend on the mist droplet density as sprayed on the wafer; larger defect counts were observed in wafer areas with more intense misting. However, the values obtained were reproducible between two wafers which were sprayed and analyzed, and usually differ by no more than 20%. Table 1 shows the added defect counts, respectively, when water, IF132, and IF169 were misted on bare Si wafers, wafers coated with PAR-817, and wafers coated with the three water-specific immersion resists. IF132 on bare Si wafers shows few added defects, consistent with good initial fluid cleanliness. The overall tendency is that the misting with high index fluids produces smaller defect counts than misting with water. This suggests that the starting point for defectivity optimization is better for the high index fluids than for water. Also note that the test itself is aggressive: the TOK TArF Pi6-001 is used with success in water-based hyper-NA scanners at low defectivity counts, but large defect counts are seen here. This makes the low defect counts for misting with the high-index liquid even more impressive.

This data gives us an initial look at fluid-resist interactions, but how these numbers translate into final imaging defects still needs some research.

Table 1. Added defect counts from misting fluid on each resist, after subtracting initial defect counts.

Fluid	Bare Si	PAR-817	Pi6-001	TAI-series	CH Resist
Water	>100,000	>100,000	>100,000	>100,000	>100,000
IF132	30	1,000	200	19,000	>100,000
IF169	1300	12,000	1,500	30,000	>100,000

### 4.3. PAG Leaching

The PAG amount that leaches from both resists into water, IF132, and IF169 was determined by puddle soaking directly on the resist surface, and then analyzing the fluids for the PAG anion by LC/MS (after PAG calibration curves were established on the instrument). Resists were spun to a thickness of 150 nm on HMDS-primed 200 mm wafers, and the edges were removed during spinning so that the resist coating diameter was 100 mm (~78 cm<sup>2</sup> surface area). After the recommended PEB for each resist, 3 mL of IF132 or IF169 was puddled over the entire resist area for 6 minutes contact time. The fluids were drained into a glass dish and collected in glass vials for analysis. For water, 15 mL was used to

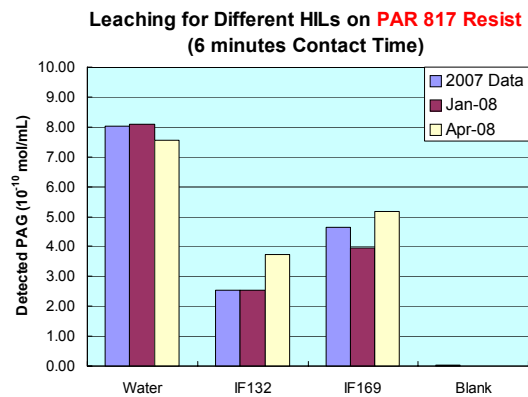


Figure 11. Amount of PAG leaching from PAR-817 in three different tests over 1 year time frame.

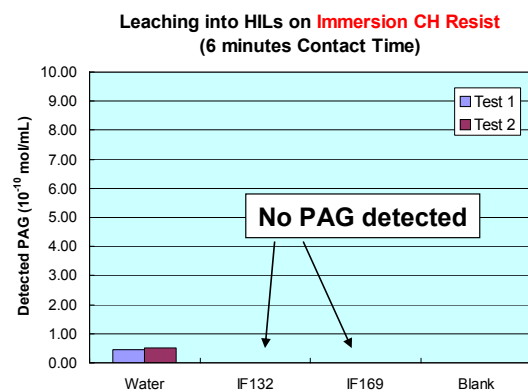
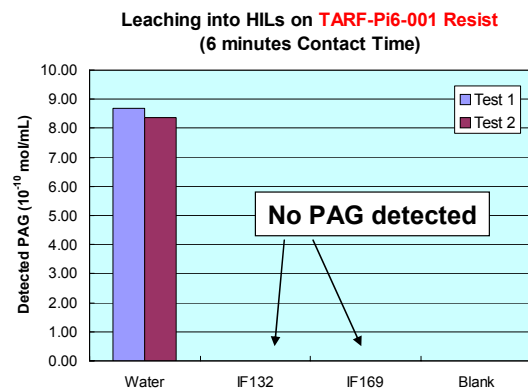


Figure 12. Amount of PAG leaching from two water-specific immersion resists into each fluid. No PAG was detected in the high index liquids.

cover the entire resist surface; so, the results obtained were multiplied by 5 to correct for this volume change. Two wafers were tested for each resist and fluid. Figure 11 shows the leaching data obtained for PAR-817 in three tests over one year apart. The results are reproducible, and show that the least PAG leaching from this resist occurs with IF132. At 6 minutes, PAG leaching is on the

order of  $3 \times 10^{-10}$  mol/mL (or  $3.2 \times 10^{-14}$  mol/cm<sup>2</sup>-sec), about two orders of magnitude lower than the upper limit specified by the stepper manufacturers (assuming PAG leaching is linear in time).

On both TArF-Pi6-001 and the water-specific immersion contact hole resist, we could not detect measurable PAG leaching into either IF132 or IF169 (Figure 12). PAG leaching from TArF-Pi6-001 into water is comparable to leaching from the dry resist PAR-817, while leaching into water from the immersion CH resist is much reduced. The reduced PAG leaching into the high index liquids with the immersion dedicated resists shows that lens contamination by PAG leaching can potentially be better controlled.

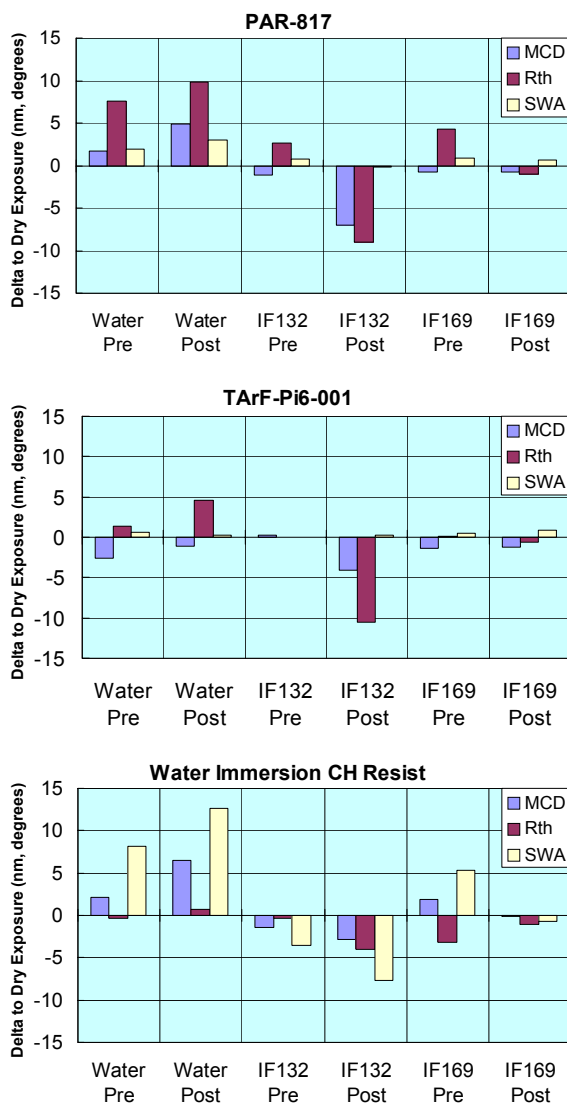


Figure 13. Delta between scatterometry parameters for a dry reference wafer and wafers soaked pre- or post-exposure. MCD = middle CD, Rth = resist thickness, and SWA = sidewall angle.

#### 4.4. Pre- and Post-soak Imaging

A resist stack consisting of 77 nm ARC29A and 150 nm of PAR-817, TArF-Pi6-001, or the water immersion CH resist was printed with 90 nm LS patterns (110 nm for the CH resist) on an ASML PAS5500/1100 (0.75 NA, 0.89-0.59 sigma outer-inner illumination). Water, IF132, or IF169 was puddled (30-40 mL for 60 seconds) over the resist and spun off (2000 rpm) during pre- or post-exposure, and average resist profiles were obtained using scatterometry metrology (KLA-T F5) after development. Figure 13 shows the delta change, in nm or degrees, of MCD (middle CD), Rth (resist thickness), and SWA (sidewall angle) of each soaking experiment, compared to dry-wafer experiments for each resist. With water, the PAR-817 resist profiles became wider and thicker in both pre- and post-exposure soaking. For TArF-Pi6-001, the profiles are more tapered, but there is also less CD and thickness change in pre- and post-exposure soaking. For the water immersion CH resist, the profiles become much less tapered under both pre- and post-exposure soak modes as compared to the dry wafer. IF132 shows the most interaction in post-exposure soaking mode in all three resists: the profiles become thinner in width and height, and for the water immersion CH resist, the profiles become more tapered, as seen in the decrease in sidewall angle. For IF169, there is less CD or thickness change in all resists, especially with post-exposure soak. Overall, the TArF-Pi6-001 resist shows less profile change for all fluids in both pre- and post-exposure soak modes. These results indicate that, even when used without a topcoat, the water-immersion dedicated resists still have good quality profiles after contact with high-index liquids. Again, this confirms the earlier findings that current water-based immersion resists are a good starting point for imaging under high index fluids.

#### 4.5. Immersion Interference Printing

A two beam interferometer was used to print line-space arrays of three resists (PAR-817, TArF-Pi6-001, and TAI-series) under the three tested fluids (water, IF132, and IF169) at 72 nm pitch. The imaging stack consisted of 130 nm TOK TILC-019 topcoat, 80 nm resist, and 40 nm Brewer ARC-29A organic BARC. Details of the experimental setup and the changes in going from water immersion to high index immersion on the interferometer have been reported elsewhere [8]. Better imaging performance was obtained with the newer water immersion resists. In some cases,

acceptable 29 nm lines were obtained at 72 nm pitch, with higher doses.

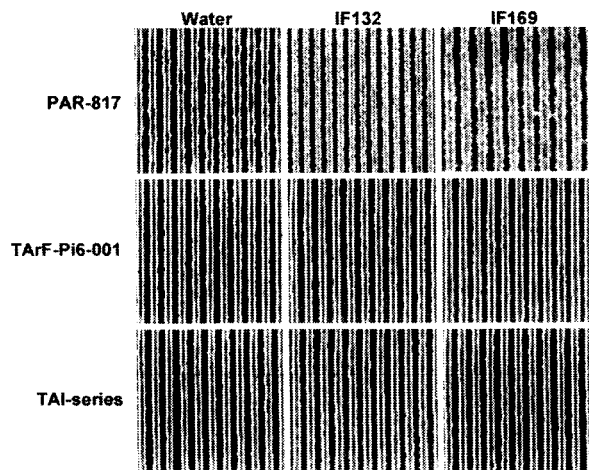


Figure 14. Top-down SEMs of 72 nm pitch lines imaged on a two beam interferometer under three liquids on three resists.

## 5. Conclusions

High-index immersion fluid technology continues to show the advances required for its manufacturing insertion. As a selected part of our total studies, we have reported here on aspects of fluid quality, fluid-resist interactions, and fluid-related radiation durability improvements. Fluid quality in terms of both soluble and insoluble impurities has been analyzed, and fluid-resist interaction studies have revealed issues related to both surface defects and imaging effects. Using immersion-specific resists can greatly reduce potential defects from such contact. Our active recycle technology leads to enhanced fluid and final lens element useful lifetimes. These are among the advances which will permit high-index immersion lithography to find its appropriate place among the approaches under consideration for patterning at 32 nm half-pitch and below. It offers improved throughput/cost versus water-immersion double patterning; and as a method (with double patterning) can extend towards 16 nm. This progression would allow time for an orderly maturing of the full set of required EUV technologies.

## Acknowledgments

The authors would like to acknowledge the assistance of Katsumi Ohmori and Junichi Onodera of TOK in the fluid-resist interactions; Vladimir Liberman, Keith Krohn and Mordechai Rothschild of MIT-Lincoln Labs; Keita Sakai, Yuichi Iwasaki and Shin-ichi Hara of Canon; Harry Sewell and Jan Mulkens of ASML; Marc

Leblans of IMEC; Paul Graupner and Ruediger Duesing of Zeiss; and Bryan Rice of Sematech in the radiation durability testing.

## Reference

1. A. Wuest, G. Hughes, Lloyd C. Litt, W. Conley, "Lithography Cost of Ownership at the 32 nm Half-Pitch Node and Beyond", *Sematech Litho Forum*, New York, May 12-14, 2008.
2. R. H. French, H. Sewell, M. K. Yang, S. Peng, D. McCafferty, W. Qiu, R. C. Wheland, M. F. Lemon, L. Markoya, M. K. Crawford, "Imaging Of 32-nm 1:1 Lines And Spaces Using 193-nm Immersion Interference Lithography With Second-Generation Immersion Fluids To Achieve A Numerical Aperture Of 1.5 And A k1 Of 0.25", *Journal of Microlithography, Microfabrication and Microsystems*, **4**, (2005) 031103.
3. S. Peng, R. H. French, W. Qiu, R. C. Wheland, M. K. Yang, M. F. Lemon, M. K. Crawford, "Second Generation Fluids for 193 nm Immersion Lithography", *Proc. SPIE Optical Microlithography XVIII*, **5754** (2005) 5754-76.
4. R. H. French, M. K. Yang, M. F. Lemon, R. A. Synowicki, G. K. Pribil, G. T. Cooney, C. M. Herzinger, S. E. Green, J. H. Burnett, S. Kaplan, "Immersion Fluid Refractive Indices Using Prism Minimum Deviation Techniques", *Proc. SPIE Optical Microlithography XVII*, **5377** (2004) 5377-173.
5. R. A. Synowicki, G. K. Pribil, G. Cooney, C. M. Herzinger, S. E. Green, R. H. French, M. K. Yang, J. H. Burnett, S. Kaplan, "Fluid Refractive Index Measurements Using Roughened Surface and Prism Minimum Deviation Techniques", *Journal of Vacuum Science And Technology B*, **22**, (2004) 3450-3.
6. R. H. French, W. Qiu, M. K. Yang, R. C. Wheland, M. F. Lemon, A. L. Shoe, D. J. Adelman, M. K. Crawford, H. V. Tran, J. Feldman, S. J. McLain, S. Peng, "Second Generation Fluids for 193nm Immersion Lithography", *Proc. SPIE Optical Microlithography XIX*, **6154** (2006) 6154-42.
7. R. H. French, V. Liberman, H. V. Tran, J. Feldman, D. J. Adelman, R. C. Wheland, W. Qiu, S. J. McLain, M. K. Yang, M. F. Lemon, L. Brubaker, A. L. Shoe, B. Fones, K. Krohn, D. Hardy, C. Y. Chen, "High Index Immersion Lithography With Second Generation Immersion

Fluids To Enable Numerical Apertures of 1.55 For Cost Effective 32 nm Half Pitches”, *Proc. SPIE Optical Microlithography XX*, **6520** (2007) 6520-59.

8. E. Hendrickx, S. Postnikov, P. Foubert, R. Gronheid, B. Kim, “Screening of Second Generation High Index Fluids”, *Proc. SPIE Advances in Resist Materials and Processing Technology XXIV*, **6519** (2007) 65190A.

9. H. V. Tran, R. H. French, D. J. Adelman, J. Feldman, W. Qiu, R. C. Wheland, L. W. Brubaker, B. E. Fischel, B. B. Fones, M. F. Lemon, M. K. Yang, O. Nagao, M. Kaku, M.

Mocella, J. J. Schmiegel, “Evaluation of Next Generation Fluids for ArF Immersion Lithography Beyond Water”, *Journal of Photopolymer Science and Technology*, **20**(5), (2007), 729-738.

10. R. H. French, H. V. Tran, D. J. Adelman, N. S. Rogado, M. Kaku, M. Mocella, C. Y. Chen, E. Hendrickx, F. Van Roey, A. S. Bernfeld, R. A. Derryberry, “High-Index Immersion Fluids Enabling Cost-Effective Single-Exposure Lithography For 32 nm Half Pitches”, *Proc. SPIE Optical Microlithography XXI*, **6924** (2008) 6924-17.